

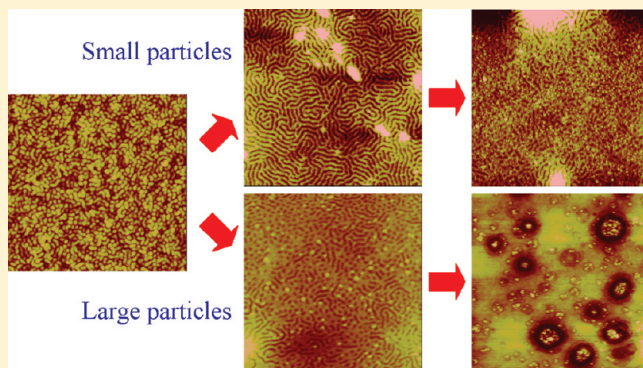
Effect of Particles on the Structure of Solvent-Annealed Block Copolymer/Nanoparticle Composite Thin Film

Chien-Chih Chang and Chieh-Tsung Lo*

Department of Chemical Engineering, National Cheng Kung University No. 1, University Road, Tainan City 701, Taiwan

 Supporting Information

ABSTRACT: The structure of nanocomposite thin films composed of polystyrene-*b*-poly(2-vinylpyridine)/Au nanoparticles (PS-PVP/Au) during chloroform vapor annealing was investigated. Our results revealed that the morphology of these composites depends on particle size and volume fraction. During solvent annealing, particles segregate to both polymer/substrate and air/polymer interfaces. The segregation of particles to the polymer/substrate interface balances the preferential interaction of two domains to the substrate, resulting in the transition of ordered domains from parallel to normal to the substrate. The introduction of large particles facilitates the segregation of particles to the top of the film. When the volume fraction of segregated particles is high, particles are repelled from the preferred domains to form particle-rich regimes. The wetting behavior of a thin film could be improved by the presence of nanoparticles. Our results showed that small particles provide the better ability to prevent thin film from dewetting.



INTRODUCTION

Block copolymers have attracted much scientific interest for the last couple of decades because block copolymers can self-assemble into rich and well-defined ordered nanostructures, including lamellae, cylinders, gyroids, and spheres, depending on their molecular weight, relative volumetric composition, and the segmental interaction parameter.^{1–5} These nanostructures of block copolymers offer a wide variety of applications, such as a reactor to synthesize nanoparticles, high-density arrays for use in data storage, photovoltaic devices, and gas separation.^{6–8} Although block copolymers exhibit potential possibilities in nanotechnology, the lack of unique properties restricts their applications. To enhance the physical properties of block copolymers, researchers are devoted to synthesizing novel block copolymer/nanoparticle composites.^{9–15} By the nature of the phase separation of block copolymer, nanoparticles can assemble into arrays in a polymer matrix. These spatially organized nanoparticles have the potential to meet the huge demands for the wide range of applications.

Many synthetic routes have been reported to tailor inorganic nanoparticles into the preferred domains of block copolymer. These methods lie in the self-assembled behavior of particles when particles are anchored to a protecting agent that has preference to one moiety of block copolymer. Further annealing provides the mobility for block copolymer to do the required work in ordering the nanoparticles in the ordered microphases of the polymer matrix. Fundamental studies on these novel composites were proposed both theoretically and experimentally to describe the phase behavior of composites as a function of molecular properties

of both polymer and particles. Schultz et al. developed the discontinuous molecular dynamics to study the phase behavior of block copolymer/nanoparticle composites.¹⁶ A copolymer was modeled as chains of tangent hard spheres with square shoulder repulsions between unlike species while nanoparticles were assumed as hard spheres with a square shoulder repulsion with one of the domains. The resulting phase diagrams were constructed as a function of particle size and interaction strength, and the phase behavior of composites exhibited lamellae, perforated lamellae, cylinders, and disordered phases. Huh et al. used a Monte Carlo simulation to investigate the effect of hard particles on the phase behavior of block copolymer.¹⁷ They found that as the size of particles became comparable to the radius of gyration of the minority block, the hybrid materials organized into a new superstructure where the particles arranged inside the copolymer micelles. This superstructure can be either stable or metastable, depending on the particle size and volume fraction. The formation of such phases is due to the interplay between the particle–particle excluded volume interaction, preferential particle/block interaction, and the enthalpic and stretching interactions within the diblock. In addition to the single-sized particles, Lee et al. investigated the self-organization of binary particle mixtures within block copolymer.¹⁸ They found that large particles localized near the center of the preferred domains due to the entropic effect between the preferred chains and particles. On the

Received: September 29, 2010

Revised: February 9, 2011

Published: March 01, 2011

other hand, small particles gained translational entropy by delocalizing and migrating into the unfavorable phase. This result revealed that the manipulation of entropy can create highly ordered nanocomposites. Chervanyov et al. used a self-consistent field theory to calculate the excess free energy upon the addition of particles in block copolymer.¹⁹ They found that both particle size and shape affected the order–disorder transition (ODT) temperature. The presence of fillers caused a significant decrease of the ODT temperature and the smaller particles exhibited a greater depression. Additionally, the effect of particle shape on the ODT temperature was calculated as a function of the aspect ratio of spherocylindrical particles. The spherocylinders with the smaller aspect ratio showed the bigger effect on the ODT. Chen and Ruckenstein investigated the dynamics of particle aggregation and the morphological evolution of block copolymer.²⁰ It was obtained that the occurrence of particle aggregation could be manipulated by particle/particle, particle/segment A, particle/segment B, and segment A/segment B interactions. As the particle/particle interaction was above a critical value, particles dispersed in the preferred domains or at the polymer/polymer interface without aggregation. On the contrary, particles showed extensive aggregation when the particle/particle interaction exceeded the critical value.

On the experimental front, Xu et al. studied the morphology of poly(methyl methacrylate) (PMMA)-grafted Fe₃O₄ nanoparticles in polystyrene-*b*-poly(methyl methacrylate) (PS-PMMA).²¹ The dispersion of nanoparticles depended strongly on the molecular weight of PMMA ligands and the greater aggregation of particles occurred with an increase in the molecular weight of PMMA. Lo et al. generated a phase diagram on block copolymer/nanoparticle composites as a function of molecular properties of polymer and particles.²² It was obtained that the dispersion of nanoparticles in the preferred domains of block copolymer caused swelling and increased the interfacial curve, leading to an order–order transition. At high particle loading, packing constraint prevented all particles assembling in the preferred domains. Thus, the excess nanoparticles were macrophase separated from the domains, inducing an order–disorder transition of polymer phase. Furthermore, the boundaries between order–order and order–disorder transitions were influenced by the relative size between particle diameter and the domain spacing of the preferred domains.²³ As particle size was comparable to the domain size, the presence of particles enhanced the local compositional fluctuations at the polymer/polymer interface. These fluctuations reduced the ability of particles to swell the preferred domains and perturbed the ordered morphology. As a result, disordered morphology of composite formed. Previous studies also demonstrated the strategy to control precisely the particle location in block copolymer domains by the manipulation of the particle volume fraction, the areal chain density of the modified particles, and the nature of ligands on particles.^{24–27} Kim et al. found that different solvent evaporation rate through a thick film caused the variation of particle distribution in depth in block copolymer/nanoparticle composites.²⁷

In comparison of bulk nanocomposites, thin film of composites is even more interesting. Different approaches have been demonstrated to incorporate nanoparticles into block copolymer thin films.^{11,12,16,28} Additionally, the physics behind these thin films was also studied.^{29–31} Hu et al. investigated the effect of 2-phenylethylthiol-coated gold nanoparticles on the morphology of PS-PMMA thin films.³⁰ It was obtained that neat block copolymer thin film formed a perpendicularly lamellar structure.

In contrast, an ordered structure disappeared with the addition of nanoparticles. Park et al. found that the morphology of a neat block copolymer thin film exhibited a parallel cylindrical structure and it transformed to a perpendicularly cylindrical structure with the addition of polyethylene-tethered gold nanoparticles.³² They further investigated the morphology of thin films as a function of humidity. During annealing, the hydrophilic nanoparticles in PMMA domains interacted with water vapor under high humidity to form an ordered structure. This strategy provides a simple route for the fabrication of ordered polymer templates without the need of a random copolymer neutralization layer while also allowing hybrid organic–inorganic materials with hierarchical order to be prepared. Spatz et al. proposed that the kinetic control of block copolymer structures was very effective in arranging nanoparticles to fabricate well-defined films containing different size of gold nanoparticles.³³ Hamdoun et al. studied a thin film containing symmetric polystyrene-*b*-polybutylmethacrylate (PS-PBMA) ($M_w = 82K$) and maghemite nanoparticles with a diameter of 3.5 nm tethered with short PS chains.³⁴ They used atomic force microscopy to characterize the variation of the lamellar spacing with different particle volume fractions and inferred that the nanoparticles were distributed throughout the PS domains rather than concentrated in the middle of the preferred domains. Lauter-Pasyuk et al. studied the same system but utilized higher molecular weight of matrix ($M_w = 135K$ and $170K$) and larger nanoparticles (4 and 6 nm).³⁵ They suggested that small particles tended to concentrate near the PS-PBMA interface while large particles concentrated in the center of the PS domains.

Although a few reports were demonstrated to address the behavior of both bulk and thin film of block copolymer/nanoparticle composite, the literature on the morphological development on the composite thin films as a function of particle size and loading during solvent annealing is scarce. In this work, we investigated the effect of particles on the structure of composite thin films under neutral vapor treatment. The polystyrene-*b*-poly(2 vinyl pyridine) (PS-PVP) and Au nanoparticles tailored with different molecular weight of thiol-terminated polystyrene (PSSH) were chosen as a model system. This study clearly shows the ordering behavior and state of particle dispersion in solvent-annealed composite thin films. We believe that this paper will be valuable to manipulate the structure of composite thin films for the potential use in nanotechnology.

EXPERIMENTAL SECTION

Materials. PS-PVP with a polydispersity index (PDI) of 1.10 was purchased from Polymer Source Inc. The number average molecular weight (M_n) of PS and PVP are 40 500 and 40 000 g/mol, respectively. This symmetric PS-PVP exhibits a lamellar structure at equilibrium (Figure S1 in Supporting Information). Hydrogen tetrachloroaurate(III) trihydrate (HAuCl₄·3H₂O, >99.99%) was purchased from Alfa Aesar and 1.0 M lithium triethylborohydride (LiB(C₂H₅)₃H) dissolved in tetrahydrofuran (THF) was provided by Aldrich Chemical Co. Thiol-terminated polystyrene with $M_n = 1500$ g/mol (PDI = 1.10), 5300 g/mol (PDI = 1.10), and 12000 g/mol (PDI = 1.09) was purchased from Polymer Source Inc.

Synthesis of PSSH-Tethered Au Nanoparticles. PSSH-tethered Au nanoparticles were synthesized by the addition of 1.0 M lithium triethylborohydride to a solution of 0.19 mmol HAuCl₄·3H₂O and 0.025 mmol PSSH in 10 mL of THF.³⁶ The

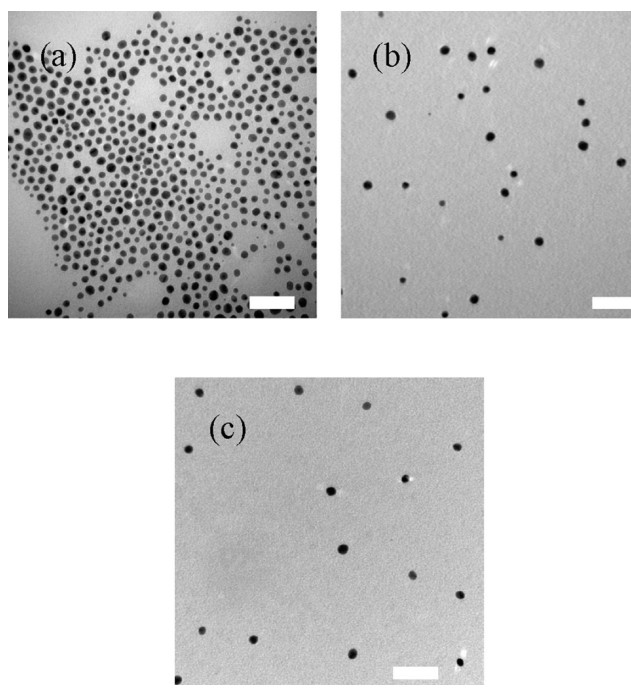


Figure 1. TEM images of Au nanoparticles tethered with different molecular weight of PSSH. (a) M_n of PSSH = 1500 g/mol; (b) M_n of PSSH = 5300 g/mol; and (c) M_n of PSSH = 12 000 g/mol. Scale bars: 50 nm.

PSSH grafts provide both good protection for nanoparticles from aggregation and the capability for particle assembly in the PS domains of PS-PVP. The particles were purified using methanol and collected by centrifuge with a spin rate of 2000 rpm.

Preparation of PS-PVP/Au Composite Thin Film. Silicon wafer was cleaned by a mixture of H_2O_2 and H_2SO_4 (30/70 v/v) solution at 100 °C for 1 h and followed by rinsing using deionized water. The wafer was dried by a purge of nitrogen gas. The PS-PVP/Au composite thin film was prepared by spin coating a solution containing 10.0 mg PS-PVP and various volume fractions of Au nanoparticles in 1.2 mL toluene at 2000 rpm. The film was dried at room temperature for 1 day and followed by another 1 day drying in vacuum to remove the residual solvent. Thin film was then annealed under various amounts of chloroform vapor (V) in a sealed bottle (60 mL) and kept at room temperature. After annealing, the resulting film was dried in vacuum for at least 1 day.

Atomic Force Microscopy (AFM). Atomic force microscopy (Digital Instrument, NS3a-2/MMAFM) was performed with a tapping mode to characterize the morphology of PS-PVP/Au composite thin films. A cantilever with a resonance frequency of 250–390 kHz and a spring constant of about 42 N/m were used. All measurements were performed at a relative set point of about 70% of free oscillation amplitude and the scan rate was in the range of 1.0–2.0 Hz. The images were taken at different areas of the same and duplicate specimen.

Transmission Electron Microscopy (TEM). The Au nanoparticles were observed by transmission electron microscopy operated on a Hitachi H7500 electron microscope. The morphology of composite thin films was also characterized by TEM. To prepare the specimen for the morphological measurement, composite thin films were spin coated on potassium bromide substrates. After solvent vapor treatment, thin films were floated

off the substrate onto water and retrieved with copper grids. To enhance the contrast between PS and PVP, PVP was selected stained by iodine vapor for 24 h. The composites were then observed using the same microscope operated at 100 kV.

Optical Microscopy. The development of dewetting of composite thin films was analyzed using a Nikon H550L Eclipse 50i optical microscope in reflection mode.

■ RESULTS AND DISCUSSION

The Characterization of Au Nanoparticles. Figure 1 shows the TEM images of Au nanoparticles tethered with different molecular weights of PSSH. The diameter of Au core with M_n of PSSH = 1500 g/mol is 7.3 ± 1.4 nm (Figure 1a). When the molecular weight of PSSH was 5300 g/mol, the Au core diameter increased to 8.5 ± 1.8 nm (Figure 1b). With further increasing molecular weight of PSSH to 12 000 g/mol, the diameter of Au core increased to 9.2 ± 1.2 nm (Figure 1c). In addition to the Au core, the PSSH shell also contributed to the size of particles. The size of the shell was interpreted by the radius of gyration (R_g) of PSSH, given by³⁷

$$R_g = \sqrt{\frac{N}{6}} b \quad (1)$$

Here N is the degree of polymerization of PSSH and b is the Kuhn length, taken as ~ 6.7 Å.³⁸ Thus, the R_g of PSSH with M_n = 1500, 5300, and 12 000 g/mol is 1.0, 1.9, and 2.9 nm, respectively. The diameter of particles including Au core and PSSH shell is 9.3, 12.3, and 15.0 nm.

Small angle X-ray scattering was also carried out to confirm the core–shell structure and size of PSSH-tethered particles (Figure S2 in Supporting Information). The data fitting using the form factor of a Schultz polydisperse core and spherical shell model³⁹ yields a mean Au core radius of 37, 46, and 54 Å and a polymer shell thickness of 8.7, 19.1, and 27.3 Å for the M_n of PSSH of 1500, 5300, and 12 000 g/mol, respectively. The mean overall diameter of PSSH tethered Au nanoparticles is then 9.1, 13.0, and 16.3 nm. The particle size obtained from two techniques showed good consistency. To make a simple description of different sized nanoparticles, we assigned the particle size (D) of 9, 12, 15 nm for different PSSH-tethered particles.

Morphology of Neat Block Copolymer Thin Film under Solvent Vapor Treatment. Figure 2 shows PS-PVP thin film prepared from toluene and treated in chloroform vapor with $V = 0.17$ mL. Because toluene is a good solvent for PS and poor solvent for PVP, the morphology of neat PS-PVP before annealing appeared a micellar structure as shown in Figure 2a. The similar morphology was also obtained in composites with particles tethered with different molecular weight of PSSH and various particle loadings. When the film was annealed in chloroform vapor for 3 h, it developed to a short striped structure with the brighter area corresponding to the PS domains and the darker background relating to the PVP phases (Figure 2b). Because of the inadequate amount of solvent to induce phase separation of PS-PVP, the film could not form well-ordered morphology and some regions in the film showed a disordered structure. After 6 h, more solvent penetrated into the film. As a result, the short stripes connected to form a continuous structure, indicating the formation of a cylindrical structure parallel to the substrate (Figure 2c). With further chloroform vapor treatment for 12 h (Figure 2d), a few small spots appeared. These spots were the

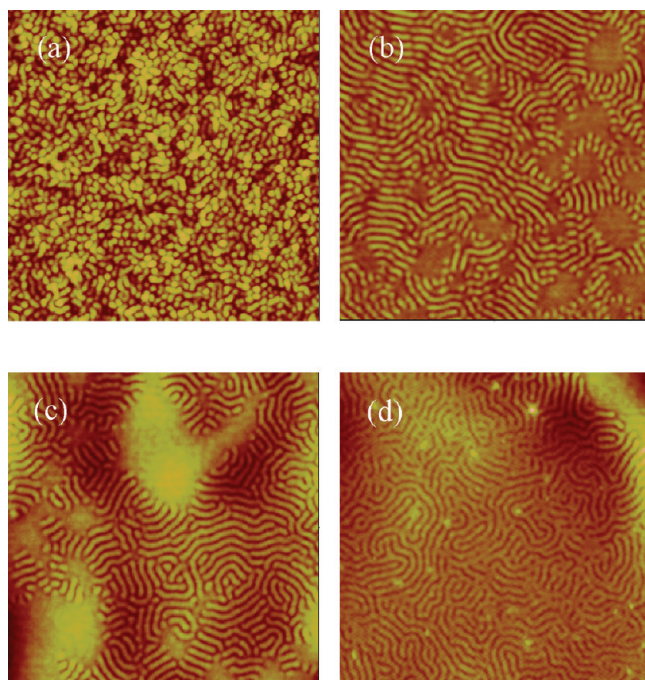


Figure 2. AFM images of PS-PVP thin films exposed to 0.17 mL chloroform vapor for different annealing time. (a) 0 h; (b) 3 h; (c) 6 h; and (d) 12 h. The image size is $2 \times 2 \mu\text{m}^2$ and the height scale is 20 nm.

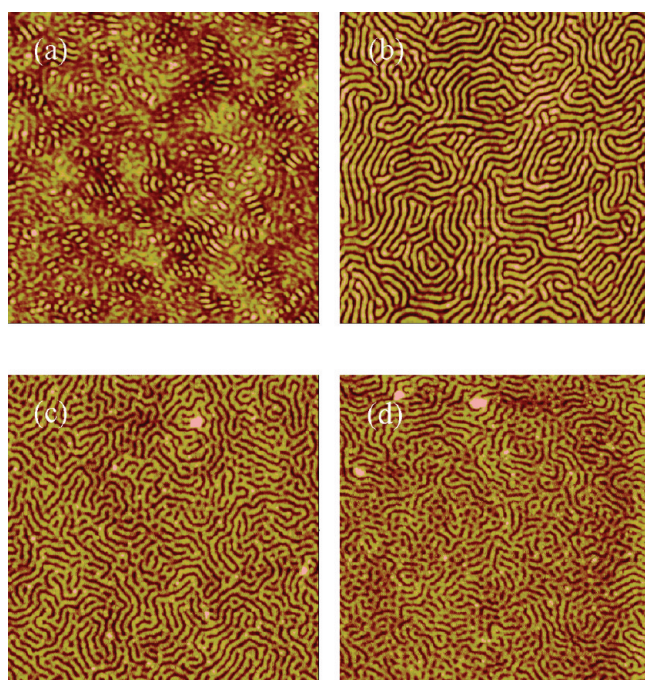


Figure 3. AFM images of nanocomposites with 1.8 vol % nanoparticles ($D = 9 \text{ nm}$) under chloroform vapor treatment ($V = 0.17 \text{ mL}$) for different annealing time. (a) 1, (b) 3, (c) 6, and (d) 12 h. The image size is $2 \times 2 \mu\text{m}^2$ and the height scale is 10 nm.

signature of the ordered cylinders normal to the substrate.^{31,40} The perpendicularly oriented cylinders form when a thin film is exposed to neutral solvent that neutralizes the preferential interaction of the substrate with the preferred block, leading to the change in the orientation of ordered domains.^{41,42}

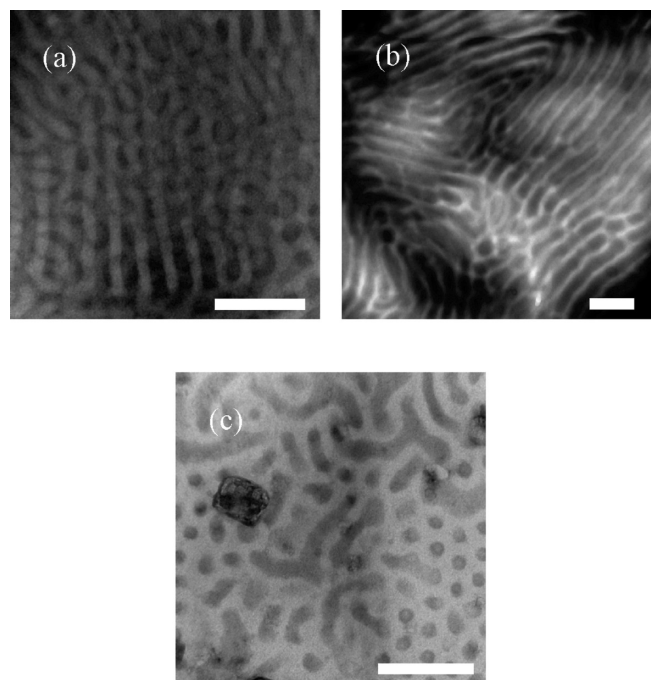


Figure 4. TEM images of nanocomposites with 1.8 vol % nanoparticles ($D = 9 \text{ nm}$) under chloroform vapor treatment ($V = 0.17 \text{ mL}$) for different annealing time. (a) 1, (b) 3, and (c) 12 h. Scale bars: 200 nm.

Effect of Particle Loading on the Morphology of Solvent-Annealed Thin Film. Figure 3 shows the AFM images of composite thin film tethered with 1.8 vol% nanoparticles with $D = 9 \text{ nm}$ for various annealing times. As thin film was treated under chloroform vapor for 1 h as shown in Figure 3a, micelles connected to form short stripes. After 3 h annealing, these short stripes developed to a continuous structure (Figure 3b). This morphological transition from short stripes to a continuous structure seems to involve mostly in the connectivity with adjacent domains with little lateral change in the structure. This process is known as a Mortensitic-type phase transition.⁴³ With increasing annealing time to 6 h (Figure 3c), a coexisted structure containing cylinders parallel and perpendicular to the substrate was formed. When thin film was exposed to chloroform vapor for 12 h, more cylinders switched their orientation normal to the substrate (Figure 3d). To confirm the morphology of these composite thin films, TEM was carried out on thin films and the results are shown in Figure 4. It appeared that longer annealing time promoted the orientational transition from parallel to perpendicular cylinders. Both AFM and TEM images showed great consistency.

The morphology of composite film with particle loading of 12.6% annealed in chloroform vapor is shown in Figure 5. The development of the film morphology was similar to the composite with particle loading of 1.8% for short annealing time. As the film was annealed for 12 h (Figure 5c), the evolution of a disordered structure occurred, resulting in a poorly ordered structure. This also caused an increase in surface roughness of the film. Additionally, some bright spots in the PS domains on the film surface were observed, indicating that particles diffused to the top of the film. This existence of particles at the air/polymer interface could facilitate the stretching of polymer chains at the air/polymer interface that would increase the conformational entropy of the film. When annealing time increased to 24 h

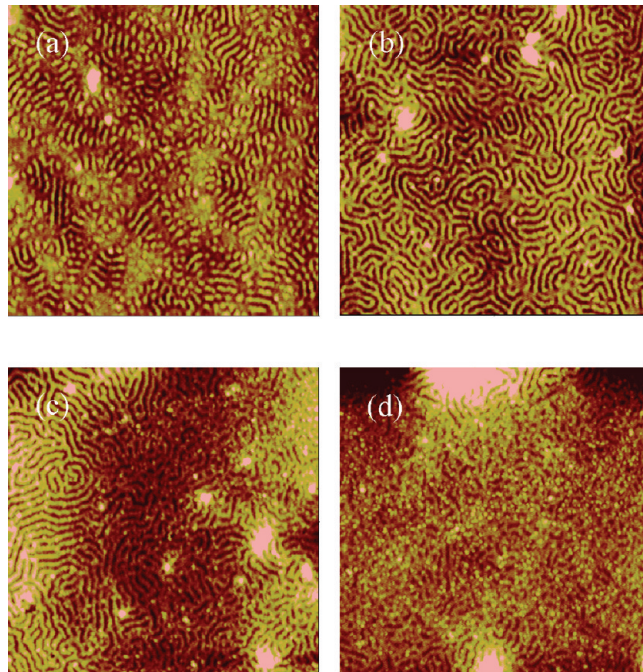


Figure 5. AFM images of nanocomposites with 12.6 vol % nanoparticles ($D = 9 \text{ nm}$) under chloroform vapor treatment ($V = 0.17 \text{ mL}$) for different annealing time. (a) 1, (b) 3, (c) 12, and (d) 24 h. The image size is $2 \times 2 \mu\text{m}^2$ and the height scale is 10 nm.

(Figure 5d), quite large numbers of particles moved to the air/polymer interface. The morphology of the film developed to a wormlike structure, losing its long-range order.

In comparison of neat block copolymer and its composite thin film, it was obtained that the presence of nanoparticles facilitates the morphological development of thin film from micelles to cylinders parallel to the substrate and continuously to a coexisted structure. This is attributed to the particles that swell the preferred domains of PS-PVP. This swelling of particles in polymer matrix promotes the disentanglements of polymer chains and hence enhances the chain mobility. This is confirmed by the reduction of the glass transition temperature from 102.7 °C for neat PS-PVP to 99.2 °C for composite with particle loading of 12.6%. The decrease of the glass transition temperature of polymer with the introduction of nanoparticles was also observed in a variety of particle sizes.²³

Effect of the Amount of Solvent on the Morphology of Solvent-Annealed Thin Film. When the amount of solvent used for vapor annealing increased to 0.77 mL, the behavior of composite thin film was dramatically different. As thin film was treated in chloroform vapor for 1 h, the morphology of thin film developed to a cylindrical structure with cylinders parallel to the substrate (Figure 6a). The evolution from a micellar structure to the cylindrical structure is much faster in comparison to the less amount of solvent ($V = 0.17 \text{ mL}$). When the amount of solvent in a controlled volume increased, the solvent vapor that penetrated into the film also increased. This enhanced the chain mobility and hence induced the phase separation of two microdomains. By prolonging the vapor exposure time to 6 h (Figure 6b), a mixed structure containing parallel and perpendicular cylinders was obtained, but the long-range arrangement became poor. By further increasing annealing time to 12 h, large holes caused by dewetting occurred as shown in Figure 6c.

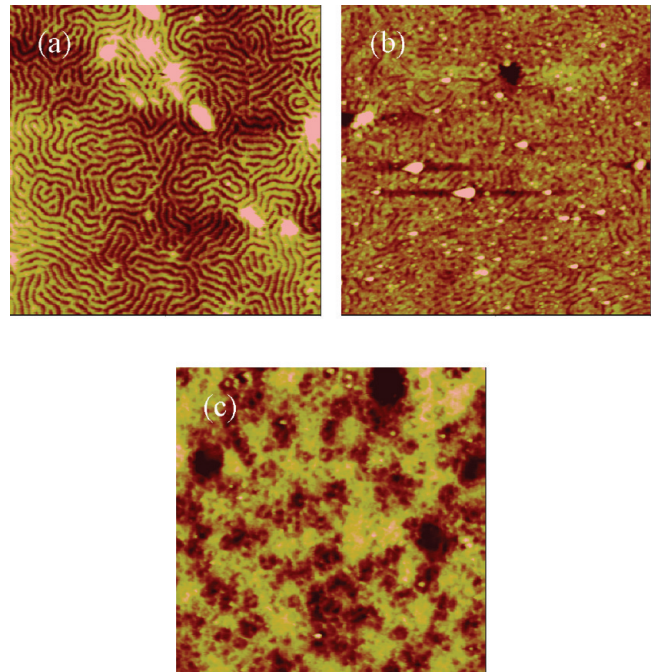


Figure 6. AFM images of nanocomposites with 12.6 vol % nanoparticles ($D = 9 \text{ nm}$) under chloroform vapor treatment ($V = 0.77 \text{ mL}$) for different annealing time. (a) 1, (b) 6, and (c) 12 h. The image size is $2 \times 2 \mu\text{m}^2$ and the height scale is 10 nm.

During solvent vapor annealing, because the entropy of solvent is much higher than that of the polymer solvent molecules prefer to condense at the polymer/substrate interface. This results in the polymer repelled from the substrate toward the free surface of the film. In addition, the high volume fraction of solvent in the film can reduce the degree of segregation of PS-PVP, leading to an increase in the compatibility of PS and PVP. These behaviors cause hole formation rather than microphase separation during solvent treatment.

Effect of Particle Size on the Morphology of Solvent-Annealed Thin Film. Figure 7 shows the morphology of composite thin film with 25.2 vol% nanoparticles ($D = 12 \text{ nm}$) annealed for various annealing times. When a film was annealed for short time (1, 3, and 6 h), a coexisted structure composed of cylinders parallel and perpendicular to the substrate was formed (Figure 7a–c). As thin film was annealed for longer time (12 and 18 h), macrophase separation of particles from polymer matrix occurred (Figure 7d,e).

The morphology of composite thin film with 28.4 vol % particles ($D = 15 \text{ nm}$) under chloroform vapor treatment is shown in Figure 8. The thin film developed to both parallel and perpendicular cylinders for 1 h (Figure 8a) and 3 h annealing (Figure 8b). Particles assembled to the top of the film were also observed. By increasing the annealing time to 6 h (Figure 8c), the aggregation of particles occurred, causing the macrophase separation of the film.

In this study, the microphase separation of composite thin film was caused by the interaction between the solvent and two domains, and the long-range repulsion is due to the incompatibility between two blocks. During neutral solvent annealing, solvent molecules swell both polymer domains to release entanglements, increasing the polymer mobility. In our system, the existence of strong polar adhesive interaction between Si substrate

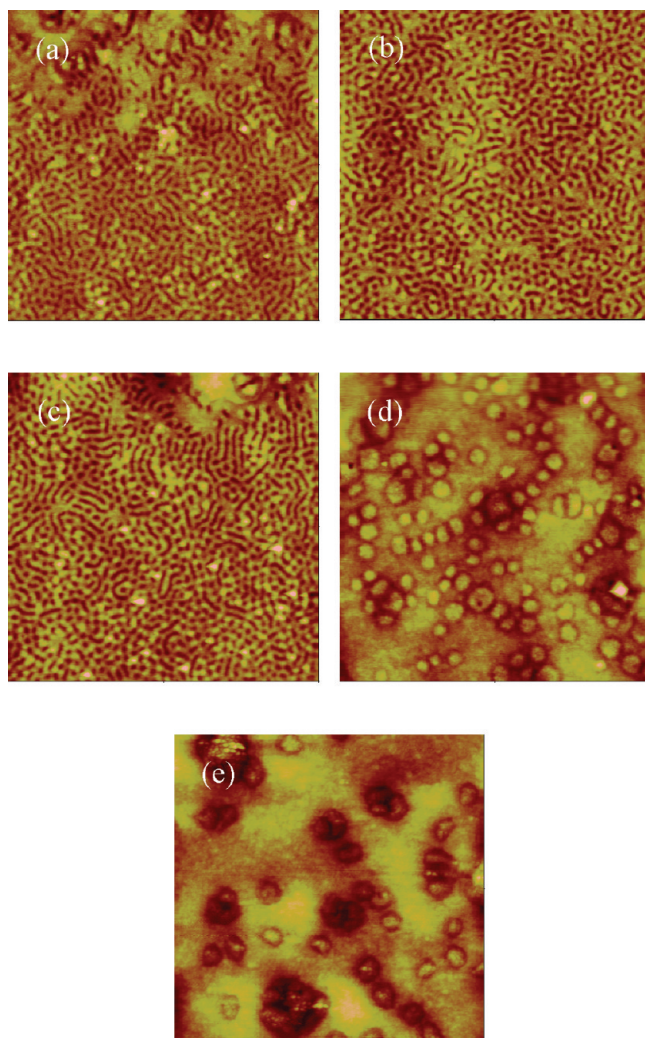


Figure 7. AFM images of nanocomposites with 25.2 vol % nanoparticles ($D = 12 \text{ nm}$) under chloroform vapor treatment ($V = 0.77 \text{ mL}$) for different annealing time. (a) 1, (b) 3, (c) 6, (d) 12, and (e) 18 h. The image size is $2 \times 2 \mu\text{m}^2$ and the height scale is 10 nm.

and PVP provides preferential interaction between PVP and substrate. In addition, the surface energy of PS ($\gamma_{\text{PS}} \sim 30 \text{ mN/m}$) is lower than that of PVP ($\gamma_{\text{PVP}} \sim 47 \text{ mN/m}$).⁴⁴ Thus, PVP preferentially locates at the polymer/substrate interface and PS stands at the air/polymer interface. However, because chloroform is a good solvent for both PS and PVP, when PS-PVP thin film is annealed in chloroform vapor the migration of PVP to the air/polymer interface also occurs.

As a thin film is further exposed to chloroform vapor, more PVP molecules move to the substrate to form a brush layer. Additionally, both PS and PVP diffuse to the air/polymer interface. This causes the development of a cylindrical structure with increasing annealing time. For short annealing time, only a small amount of solvent diffuses into the film and fully ordered morphology could not be obtained. As annealing time increases, solvent molecules promote chain mobility and composite thin film develops to an ordered structure. We further discovered that the incorporation of particles into the preferred domains of block copolymer facilitates the orientational transition of ordered domains regardless of the particle size. It was suggested that the change in the orientation of ordered domains with the

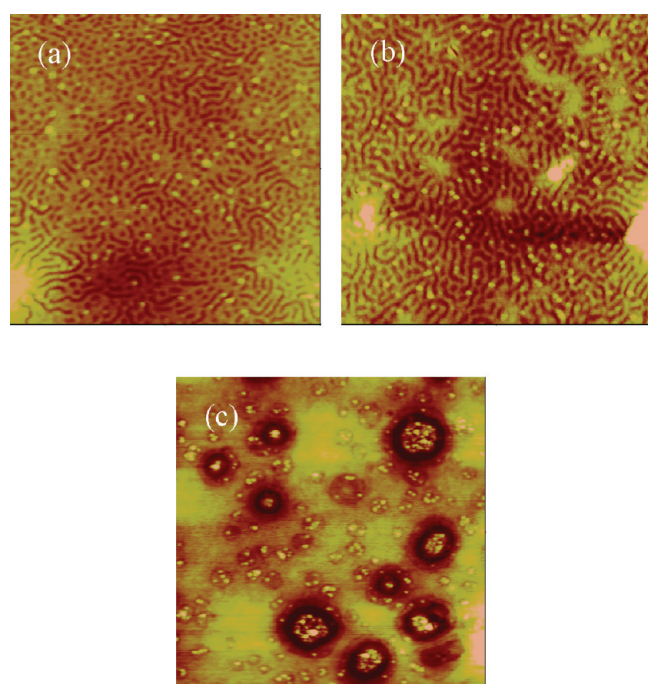


Figure 8. AFM images of nanocomposites with 28.4 vol % nanoparticles ($D = 15 \text{ nm}$) under chloroform vapor treatment ($V = 0.77 \text{ mL}$) for different annealing time. (a) 1, (b) 3, and (c) 6 h. The image size is $2 \times 2 \mu\text{m}^2$ and the height scale is 10 nm.

presence of nanoparticles was attributed to the nanoparticles that effectively balance the surface interactions between two domains.³¹ In our study, the low surface energy PS coated with even the lower surface energy of PSSH-tethered Au nanoparticles could not balance the surface interactions relative to the high surface energy PVP domains (γ_{PS} of PSSH with molecular weight of 1500, 5300, and 12 000 g/mol is 27.13, 28.74, and 29.26 mN/m respectively, calculated from $\gamma_{\text{PS}} = 29.97 - (372.7/M_n^{2/3})^{45}$). Thus, the ordering behavior in our work cannot be interpreted by Lin's expression. Kim and Green investigated the phase behavior of thin film containing brush-coated nanoparticles/homopolymer mixtures.⁴⁶ When the degree of polymerization of the homopolymer host is much larger than that of the grafted chains, nanoparticles segregate exclusively at the substrate and free surface. In our block copolymer/nanoparticle composite thin film, the molecular weight of block copolymer is much larger than that of the grafted chains. Thus, the particle segregation occurs. This segregation of particles to the polymer/substrate interface significantly reduces the preferential interaction of PVP to the substrate, allowing the PS movement to the polymer/substrate interface. This behavior forces the orientation of ordered domains from parallel to perpendicular.

In comparison of the composite film with the introduction of different-sized particles, the segregation of particles to the air/polymer interface was promoted when large particles were sequestered in the preferred domains. This was supported by the composites with particle size of 15 nm annealed for 1 h in Figure 8a. In contrast, small particles took longer time to move to the air/polymer interface. It was suggested that large particles are confined at the center of the preferred domains whereas small particles disperse uniformly within the corresponding domains.⁴⁷ When particles are located at the center of the domains, the particle-particle distance is small especially when particle volume

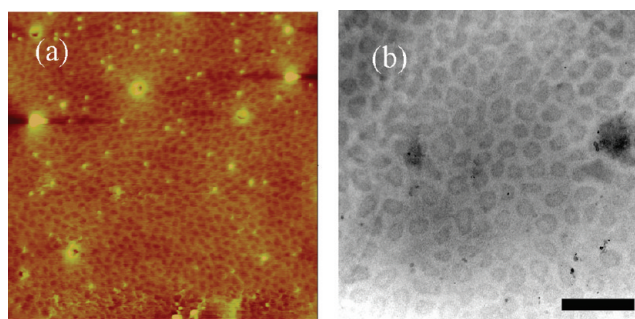


Figure 9. AFM images of nanocomposites with the addition of 10 vol % PS homopolymer under chloroform vapor treatment ($V = 0.77 \text{ mL}$). (a) 1.8 vol % particles ($D = 9 \text{ nm}$); (b) the corresponding TEM image; and (c) 25.2 vol % particles ($D = 12 \text{ nm}$). The AFM image size is $2 \times 2 \mu\text{m}^2$ and the height scale is 10 nm. The scale bar in TEM image is 200 nm.

fraction is high. The confinement of the chains between nanoparticles reduces the conformational entropy of the host chains. This favors the particles to be repelled from the host. Additionally, as we mentioned that particles in composite thin film tend to segregate to the air/polymer and substrate/polymer interfaces. These two effects force large particles to move to the top of the film. On the contrary, small particles disperse uniformly in the preferred domains and the particle–particle distance is much larger. Thus, the loss of conformal entropy due to the confinement of host chains between particles is less. Although particles still have a tendency to move to the air/polymer interface, the driving force is much smaller. Thus, the particle diffusion to the air/polymer interface is slower as seen in Figure 7 that only small number of particles segregates to the top of the film for 6 h annealing.

In Figure 7d,e and Figure 8c, long time annealing induced huge particle aggregation. In the bulk composites, particles are well organized in the PS domains of PS-PVP. After the segregation of particles occurs, particles move to the PS domains at top of the film, causing the increasing local volume fraction of particles. This behavior enhances the local concentration fluctuation and hence the interfacial roughness between two domains, resulting in the distortion in the morphology as shown in Figure 5d. As the number of segregated particles at top of the film exceeds the threshold particle loading in the PS domains, the excess particles cannot assemble in the PS domains and the system undergoes particle aggregation to release the stretching energy in the corresponding domains.

It has to point out that the complete orientation of ordered domains can be achieved by the introduction of small molecular weight of PS homopolymer (hPS, $M_n = 2400 \text{ g/mol}$) in composite thin film. This hPS homopolymer can reduce the

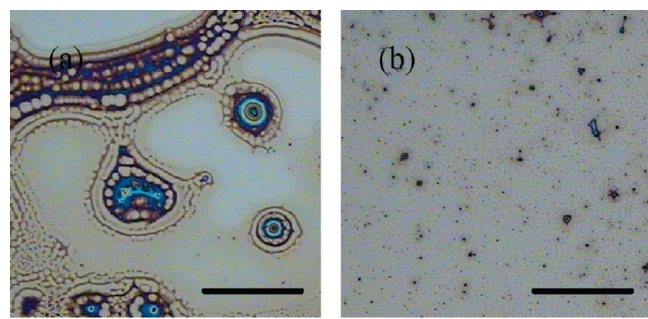


Figure 10. OM images of nanocomposite treated under chloroform vapor ($V = 0.77 \text{ mL}$) for 3 h. (a) Neat PS-PVP and its composites with particle size of (b) 9 nm, (c) 12 nm, and (d) 15 nm. Scale bars: 100 μm .

stretched chains caused by the nanoparticles and hence improve the ordering of composite thin film. Figure 9a,b shows the morphology of composite thin film with the addition of 10 vol % hPS. The cylinders normal to the substrate were observed. Although the presence of hPS facilitates the orientational transition of ordered domains of composite thin film, it seems not to be efficient when the content of nanoparticle is high or the particle size is large. In Figure 9c, the huge segregation of particles to the air/polymer interface occurred, resulting in the disordering of composite thin film.

Dewetting of Composite Thin Film. In addition to the ordered behavior of thin films, according to the studies of the homopolymer/nanoparticle hybrid materials and homopolymer/homopolymer blend films, the addition of particles or homopolymers in a thin film can effectively inhibit the dewetting phenomenon.^{48–54} In our study, we also characterized the dewetting of composite thin films by optical microscopy and the images are shown in Figure 10. Figure 10a shows extensive dewetting of a neat PS-PVP thin film exposed to solvent vapor for 3 h. The introduction of nanoparticles with $D = 9 \text{ nm}$ significantly reduced the dewetted area (Figure 10b). As $D = 12 \text{ nm}$, the dewetted area, consisting of a hole surrounded by rim, was formed (Figure 10c). The formation of the rim is due to the expelling of materials from the center of a hole into the rim at the edges of the hole. With further increasing particle size to 15 nm, holes impinged and coalesced to form interpenetrating phases (Figure 10d). On the basis of the structure of dewetting from OM, we analyzed the size of the dewetted area prior to the hole impingement by the measurement of the hole diameter and the results are shown in Figure 11. It has to point out that neat PS-PVP thin film formed interpenetrating phases after 10 min annealing. When nanoparticles with $D = 9 \text{ nm}$ were introduced to the film, dewetting occurred through the formation of small holes for short annealing time and prolonged annealing time did

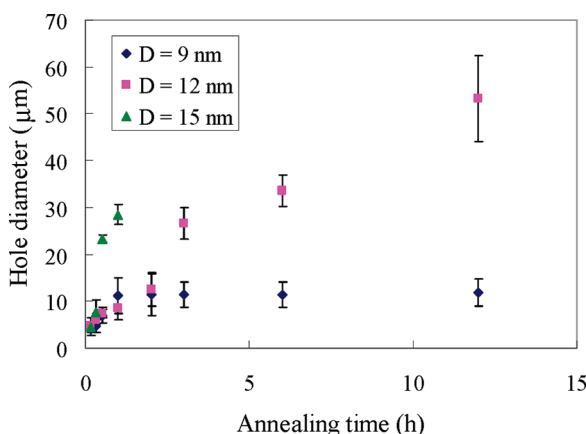


Figure 11. The diameter of dewetted area in composites as a function of solvent annealing time (particle volume fraction $\sim 20\%$).

not alter the morphology of the structure to any major extent. As the particle size increased to 12 nm, the size of the dewetted area increased continuously with time and the diameter of holes reached to $53 \mu\text{m}$ after 12 h annealing. Further increasing particle size to 15 nm caused extensive dewetting and holes impinged after 1 h annealing. From the results, it was obtained that the dewetting of thin film was inhibited by the addition of the PSSH tethered nanoparticles. The ability of preventing film from dewetting enhanced as the particle size decreased. Luo and co-workers demonstrated that the wetting of thin film reduced as the particle size increased.⁴⁹ Jayaraman et al. utilized the generalized microscopic polymer reference interaction site model (PRISM) theory to study the structure and phase behavior of polymer-tethered spherical nanoparticles in a dense homopolymer melt.⁵⁰ They found that dewetting enhanced when nanoparticles were tethered with short chains and the wetting of film improved when nanoparticles were attached with long chains. This behavior was interpreted by the diminishing of effectiveness of grafted chains in promoting dispersion when the volume of particles becomes much larger than that of the tethered chains.⁵⁵ In our system, the particle size increased with an increase in the PSSH chain length. Thus, the dewetting of composite thin film was caused by the competition between particle size and PSSH chain length. Because the wetting of composite thin film reduced with an increased in total particle size, it indicates that the particle size effect on the wetting of composite film dominates the chain length effect.

CONCLUSION

The morphological development of thin films of PS-PVP/Au composites under chloroform vapor treatment was studied using both AFM and OM. The structure of these composite thin films showed a strong function of the particle concentration and size, and the amount of solvent used for annealing. It was obtained that the introduction of nanoparticles in block copolymer swells the preferred domains that facilitates the development of ordered domains. In addition, nanoparticles also promote the orientational transition of ordered domains from parallel to perpendicular to the substrate. This is attributed to the segregation of particles to the polymer/substrate interface that effectively balances the preferential interactions of both domains to the substrate, leading to the orientational transition of ordered domains. During solvent annealing, the segregation of particles

to the air/polymer interface is also observed. For large particles, the confinement of particles in the center of the preferred domains causes a reduction of the conformational entropy of the corresponding domains. As a result, the segregation of particles to the air/polymer interface is enhanced when large particles are incorporated into the preferred domains. This segregation of nanoparticles to the top of the film increases the local concentration of particles in the PS domains, causing an increase in surface roughness and hence the formation of a disordered structure. As the available volume in the PS domains saturates, particles aggregate to form macrophase separation.

Under solvent vapor treatment, solvent induces dewetting of thin film. The dewetting of thin film could be effectively reduced by the addition of nanoparticles. The ability to reduce the dewetting of thin film using nanoparticles is affected by the competition between particle size and grafted chain length. Because the wetting of a thin film is improved by the introduction of small particles, it suggests that the particle size effect suppresses the chain length effect.

ASSOCIATED CONTENT

S Supporting Information. Details on the morphology of neat PS-PVP and the SAXS measurement and the data fitting of synthesized Au nanoparticles using a spherical shell model. This material is available free of charge via the Internet at <http://pubs.acs.org>.

AUTHOR INFORMATION

Corresponding Author

*E-mail: tsunglo@mail.ncku.edu.tw. Tel: +886-6-2757575 ext 62647. Fax: +886-6-2344496.

ACKNOWLEDGMENT

This work is funded by National Science Council in Republic of China under Grant NSC 98-2221-E-006-004-MY2.

REFERENCES

- (1) Bates, F. S.; Fredrickson, G. H. *Annu. Rev. Phys. Chem.* **1990**, *41*, 525–557.
- (2) Fasolka, M. J.; Mayes, A. M. *Annu. Rev. Mater. Res.* **2001**, *31*, 323–355.
- (3) Matsen, M. W.; Bates, F. S. *Macromolecules* **1996**, *29*, 1091–1098.
- (4) Tanaka, H.; Hasegawa, H.; Hashimoto, T. *Macromolecules* **1991**, *24*, 240–251.
- (5) Vavasour, J. D.; Whitmore, M. D. *Macromolecules* **1992**, *25*, 5477–5486.
- (6) Cohen, R. E. *Curr. Opin. Solid State Mater. Sci.* **1999**, *4*, 587–590.
- (7) Förster, S.; Antonietti, M. *Adv. Mater.* **1998**, *10*, 195–217.
- (8) Xuan, Y.; Peng, J.; Cui, L.; Wang, H.; Li, B.; Han, Y. *Macromolecules* **2004**, *37*, 7301–7307.
- (9) Aizawa, M.; Buriak, J. M. *Chem. Mater.* **2007**, *19*, 5090–5101.
- (10) Boontongkong, Y.; Cohen, R. E. *Macromolecules* **2002**, *35*, 3647–3652.
- (11) Melde, B. J.; Burkett, S. L.; Xu, T.; Goldbach, J. T.; Russell, T. P.; Hawker, C. J. *Chem. Mater.* **2005**, *17*, 4743–4749.
- (12) Misner, M. J.; Skaff, H.; Emrick, T.; Russell, T. P. *Adv. Mater.* **2003**, *15*, 221–224.
- (13) Spatz, J. P.; Herzog, T.; Mossmer, S.; Ziermann, P.; Moller, M. *Adv. Mater.* **1999**, *11*, 149–153.
- (14) Zhang, Q. L.; Xu, T.; Butterfield, D.; Misner, M. J.; Ryu, D. Y.; Emrick, T.; Russell, T. P. *Nano Lett.* **2005**, *5*, 357–361.

- (15) Zou, S.; Hong, R.; Emrick, T.; Walker, G. C. *Langmuir* **2007**, *23*, 1612–1614.
- (16) Schultz, A. J.; Hall, C. K.; Genzer, J. *Macromolecules* **2005**, *38*, 3007–3016.
- (17) Huh, J.; Ginzburg, V. V.; Balazs, A. C. *Macromolecules* **2000**, *33*, 8085–8096.
- (18) Lee, J. Y.; Thompson, R. B.; Jasnow, D.; Balazs, A. C. *Faraday Discuss.* **2003**, *123*, 121–131.
- (19) Chervanyov, A. I.; Balazs, A. C. *J. Chem. Phys.* **2003**, *119*, 3529–3534.
- (20) Chen, H.; Ruckenstein, E. *J. Chem. Phys.* **2009**, *131*, 244904.
- (21) Xu, C.; Ohno, K.; Ladmiral, V.; Composto, R. J. *Polymer* **2008**, *49*, 3568–3577.
- (22) Lo, C. –T.; Lee, B.; Pol, V. G.; Dietz Rago, N. L.; Seifert, S.; Winans, R. E.; Thiagarajan, P. *Macromolecules* **2007**, *40*, 8302–8310.
- (23) Lo, C. –T.; Chang, Y. –C.; Wu, S. –C.; Lee, C. –L. *Colloids Surf, A* **2010**, *368*, 6–12.
- (24) Chiu, J. J.; Kim, B. J.; Kramer, E. J.; Pine, D. J. *J. Am. Chem. Soc.* **2005**, *127*, 5036–5037.
- (25) Chiu, J. J.; Kim, B. J.; Yi, G. R.; Bang, J.; Kramer, E. J.; Pine, D. J. *Macromolecules* **2007**, *40*, 3361–3365.
- (26) Kim, B. J.; Bang, J.; Hawker, C. J.; Kramer, E. J. *Macromolecules* **2006**, *39*, 4108–4114.
- (27) Kim, B. J.; Given-Beck, S.; Bang, J.; Hawker, C. J.; Kramer, E. J. *Macromolecules* **2007**, *40*, 1796–1798.
- (28) Pietsch, T.; Metwalli, E.; Roth, S. V.; Gebhardt, R.; Gindy, N.; Müller-Buschbaum, P.; Fahmi, A. *Macromol. Chem. Phys.* **2009**, *210*, 864–878.
- (29) He, J.; Tangirala, R.; Emrick, T.; Russell, T. P.; Boker, A.; Li, X.; Wang, J. *Adv. Mater.* **2007**, *19*, 381–385.
- (30) Hu, S. W.; Brittain, W. J.; Jacobson, S.; Balazs, A. C. *Eur. Polym. J.* **2006**, *42*, 2045–2052.
- (31) Lin, Y.; Boker, A.; He, J.; Sill, K.; Xiang, H.; Abetz, C.; Li, X.; Wang, J.; Emrick, T.; Long, S.; Wang, J.; Balazs, A.; Russell, T. P. *Nature* **2005**, *434*, 55–59.
- (32) Park, S. C.; Kim, B. J.; Hawker, C. J.; Kramer, E. J.; Bang, J.; Ha, J. S. *Macromolecules* **2007**, *40*, 8119–8124.
- (33) Spatz, J. P.; Roescher, A.; Moller, M. *Adv. Mater.* **1996**, *8*, 337–340.
- (34) Hamdoun, B.; Ausserre, D.; Cabuil, V.; Joly, S. *J. Phys. II* **1996**, *6*, 503–510.
- (35) Lauter-Pasyuk, V.; Lauter, H. J.; Ausserre, D.; Gallot, Y.; Cabuil, V.; Kornilov, E. I.; Hamdoun, B. *Physica B* **1997**, *241*, 1092–1094.
- (36) Yee, C. K.; Jordan, R.; Ulman, A.; White, H.; King, A.; Rafailovich, M.; Sokolov, J. *Langmuir* **1999**, *15*, 3486–3491.
- (37) de Gennes, P. G. *Scaling Concepts in Polymer Physics*; Cornell University Press: Ithaca, NY, 1979.
- (38) Russ, T.; Brenn, R.; Abel, F.; Boue, F.; Geoghegan, M. *Eur. Phys. J. E* **2001**, *4*, 419–433.
- (39) Bartlett, P.; Ottewill, R. H. *J. Chem. Phys.* **1992**, *96*, 3306–3318.
- (40) Tung, S. –H.; Kalarickal, N. C.; Mays, J. W.; Xu, T. *Macromolecules* **2008**, *41*, 6453–6462.
- (41) Hawker, C. J.; Russell, T. P. *MRS Bull.* **2005**, *30*, 952–966.
- (42) Kim, S. H.; Misner, M. J.; Xu, T.; Kimura, M.; Russell, T. P. *Adv. Mater.* **2004**, *16*, 226–231.
- (43) Breulmann, M.; Forster, S.; Antonietti, M. *Macromol. Chem. Phys.* **2000**, *201*, 204–211.
- (44) Brandrup, J.; Immergut, E. H. *Polymer Handbook*, 3rd ed.; John Wiley & Sons: New York, 1998.
- (45) Wu, S. *Polymer interface and adhesion*; Marcel Dekker: New York, 1982.
- (46) Kim, J.; Green, P. F. *Macromolecules* **2010**, *43*, 1524–1529.
- (47) Thompson, R. B.; Ginzburg, V. V.; Matsen, M. W.; Balazs, A. C. *Science* **2001**, *292*, 2469–2472.
- (48) Sharma, S.; Rafailovich, M. H.; Peiffer, D.; Sokolov, J. *Nano Lett.* **2001**, *1*, 511–514.
- (49) Luo, H. B.; Gersappe, D. *Macromolecules* **2004**, *37*, 5792–5799.
- (50) Jayaraman, A.; Schweizer, K. S. *Macromolecules* **2008**, *41*, 9430–9438.
- (51) Krishnan, R. S.; Mackay, M. E.; Hawker, C. J.; Van Horn, B. *Langmuir* **2005**, *21*, 5770–5776.
- (52) Holmes, M. A.; Mackay, M. E.; Giunta, R. K. *J. Nanopart. Res.* **2007**, *9*, 753–763.
- (53) Lan, Q.; Francis, L. F.; Bates, F. S. *J. Polym. Sci., Polym. Phys. Ed.* **2007**, *45*, 2284–2299.
- (54) Barnes, K. A.; Karim, A.; Douglas, J. F.; Nakatani, A. I.; Gruell, H.; Amis, E. J. *Macromolecules* **2000**, *33*, 4177–4185.
- (55) Jayaraman, A.; Schweizer, K. S. *J. Chem. Phys.* **2008**, *128*, 164904.